Application of artificial neural networks to the evaluation of the ultimate strength of uniaxially compressed welded stiffened aluminium plates

Mohammad Reza Zareei, Mohammad Reza Khedmati and Philippe Rigo

Proceedings of the Institution of Mechanical Engineers, Part M: Journal of Engineering for the Maritime Environment 2012
226: 197 originally published online 1 June 2012
DOI: 10.1177/1475090212445865

Original Article

Institution of MECHANICAL ENGINEERS

Journal of ENGINEERING FOR THE MARITIME ENVIRONMENT

Proc IMechE Part M: J Engineering for the Maritime Environment
226(3) 197–213

DOI: 10.1177/1475090212445865
pim.sagepub.com
SAGE

Application of artificial neural networks to the evaluation of the ultimate strength of uniaxially compressed welded stiffened aluminium plates

Mohammad Reza Zareei[1], Mohammad Reza Khedmati[2] and Philippe Rigo[3]

Abstract

A series of elastoplastic large-deflection finite element analyses is performed on stiffened aluminium plates with flat-bar stiffeners under in-plane longitudinal compression loads. Then, the closed-form ultimate compressive strength formula is derived for stiffened aluminium plates by regression analysis. Finally, artificial neural network methodology is applied to predict the ultimate strength of uniaxially compressed stiffened aluminium plates. It is found that artificial neural network models can produce a more accurate prediction of the ultimate strength of the stiffened aluminium plates than can the existing empirical formula.

Keywords

Ultimate strength, stiffened aluminium plates, axial compression, empirical formulation, heat-affected zone, finite element method, artificial neural networks

Date received: 6 June 2011; accepted: 16 March 2012

Introduction

Stiffened plates are basic building elements in many civil as well as marine structural applications and, as such, accurate strength assessment of individual stiffened plate components is one of the key parameters required to perform a general ultimate strength analysis of the global structure. These components are generally subjected to a variety of either in-plane or out-of-plane loads, among which in-plane compression plays a dominant role.

Four different approaches are usually applied in order to estimate the ultimate strength of stiffened plates. These are experimental studies, numerical methods, empirical formulations and analytical methods. Experiments are normally very expensive and thus they are used at the final stages in order to validate the results of other methods. Numerical methods are very widely used, but their applications need sufficient knowledge of the method, its applicability and relevant modelling features. Also, often the lack of time limits the use of both experimental and numerical methods for predicting the ultimate strength of stiffened plates. As a result, empirical and also analytical formulations are often preferred. Most of the available empirical formulations are based upon regression analyses, and the analytical rational methods are based on the principles of structural mechanics. Some key important parameters are involved in these formulations.

The ultimate strength design formulae available for stiffened steel plates cannot be directly applied to stiffened aluminium plates even though the corresponding material properties are properly accounted for. This is partly because the constitutive stress–strain relationship of aluminium alloys is different from that of structural steel. Strain hardening in the elastic–plastic range after

[1]Chabahar Maritime University, Chabahar, Iran
[2]Department of Marine Technology, Amirkabir University of Technology, Tehran, Iran
[3]ANAST, University of Liège, Liège, Belgium

Corresponding author:
Mohammad Reza Khedmati, Department of Maritime Engineering, Amirkabir University of Technology, 424 Hafez Avenue, Tehran 15914, Iran.
Email: khedmati@aut.ac.ir

the proportional limit has a significant influence on the ultimate load behaviour of aluminium structures, whereas the elastic–perfectly plastic material model is well adapted to steel structures. Also, softening in the heat-affected zone (HAZ) significantly affects the ultimate strength behaviour of aluminium structures, whereas its effect on steel structures is of very little importance.

The ultimate strength of stiffened steel plates has been the subject of many investigations, both experimentally[1–5] and numerically,[6–10] with the most significant contributions in the field of ship structures and bridges. The literature on stiffened aluminium plates is more limited. Clarke and Narayan[11] reported buckling tests on an aluminium alloy AA5083 plate with welded T-bar and flat-bar stiffeners. Their experimental programme consisted of eight compression tests on panels with different plate and stiffener sizes, with buckling over two spans as the failure mode. The ultimate strength of stiffened aluminium alloy AA6082-T6 plates under axial compression was investigated by Aalberg et al.[12,13] using numerical and experimental methods. Kristensen and Moan[14] demonstrated numerically the effect of the HAZ and the residual stresses on the ultimate strength of rectangular aluminium alloy (AA5083 and AA6082) plates under biaxial loading of the plates. Some initial experimental and numerical simulations on the torsional buckling of flat bars in aluminium panels have also been presented by Zha and co-workers.[15–17] Hopperstad et al.[18] carried out a study with the objective of assessing the reliability of non-linear finite element analyses in predictions on the ultimate strength of aluminium plates subjected to in-plane compression. Rigo et al.[19] made a numerical investigation to present reliable finite element models to study the behaviour of axially compressed stiffened aluminium panels (including extruded profiles).

Among the most recent studies, reference can be made to the work of Paik et al.[20] on the subject of the ultimate limit state design of multi-hull ships made in aluminium. The impact of initial imperfections due to fusion welding on the ultimate strength of stiffened aluminium plates was studied by Paik et al.[21] and Collette.[22] Paik et al.[21] defined the fabrication-related initial imperfections of fusion-welded stiffened aluminium plate structures at three levels. Also, Paik[23] derived empirical formulations for predicting the ultimate strength of stiffened aluminium plates under axial compression. Future trends and research needs in aluminium structures were outlined by Sielski.[24] Mechanical collapse tests on stiffened aluminium structures for marine applications were performed by Paik et al.[25,26] Recently, Paik[27] studied the buckling collapse testing of friction-stir-welded aluminium stiffened plate structures.

Most recently, Khedmati et al.[28] carried out an extensive sensitivity analysis on the buckling and ultimate strength of continuous stiffened aluminium plates under combined in-plane compression and different lateral pressures. They finally derived a set of empirical formulations based on regression analyses in order to predict the ultimate strength of stiffened aluminium plates.[29]

Zanic et al.[30] presented a design environment for the structural design of ships. They showed the usefulness of the environment in the structural design of modern multi-deck ships at the conceptual design stage.

Artificial neural network (ANN) methods have been successfully applied by Pu and co-workers[31–33] to estimate the ultimate compressive strength of uncorroded and pitted steel plates, a very important problem in the field of naval architecture. Sadovský and Guedes Soares[34] developed an ANN model in order to predict the ultimate strength of thin rectangular plates with weld-induced initial imperfections.

To the knowledge of the present authors, ANN methods have not so far been examined for the strength assessment of stiffened aluminium plates. Thus the main aim in the present paper is to apply ANN methodology in order to predict the ultimate strength of uniaxially compressed stiffened aluminium plates. To achieve this aim, first a series of elastoplastic large-deflection finite element analyses is performed on stiffened aluminium plates. A database consisting of the main characteristics of the analysed models is summarized, focusing on the obtained ultimate strength values. Then, a regression-based formulation is introduced in order to assess the ultimate strength of the analysed models. Finally, an ANN model is generated for predicting the ultimate compressive strength of the stiffened aluminium plates. The accuracy of the ANN model is checked against the regression-based empirical formulation.

Numerical database of the ultimate strength values

Structural arrangements and geometrical characteristics of stiffened aluminium plates

The geometrical characteristics of the analysed stiffened plates are given in Table 1. All analysed stiffened aluminium plates have flat-bar stiffeners, as shown in Figure 1. The geometrical characteristics are chosen so that a wide variety of stiffness values can be considered.

Finite element code and adopted elements

The collapse behaviour and ultimate strength of stiffened aluminium plates are hereby assessed using ANSYS,[35] in which both the material and the geometric non-linearities are taken into account. Among the library of the available elements of the ANSYS finite element method (FEM) program, the four-node SHELL43 and eight-node SHELL181 elements are used for the mesh of the stiffened plate models when neglecting the welding residual stresses and assuming the welding residual stresses respectively. In each case, 300 elements are used to model each local plate panel (the

Table 1. Summary of the ultimate strength of the continuous stiffened aluminium plates obtained by the FEM, empirical formulation and ANN (stiffener type, flat bar; without lateral pressure).

Stiffener type	ID	a (mm)	b (mm)	t (mm)	h_w (mm)	t_w (mm)	β	λ	$\left(\frac{\sigma_{Ult}}{\sigma_{Yseq}}\right)_{FEM}$	$\left(\frac{\sigma_{Ult}}{\sigma_{Yseq}}\right)_{Empiricalformula}$	$\left(\frac{\sigma_{Ult}}{\sigma_{Yseq}}\right)_{Paik}$	$\left(\frac{\sigma_{Ult}}{\sigma_{Yseq}}\right)_{ANN}$
Flat bar	1	1200	160	10	40	4	0.972	1.373	0.734	0.816	0.411	0.7738
Flat bar	2	1200	160	10	65	5	0.972	0.714	0.829	0.787	0.617	0.8388
Flat bar	3	1200	160	10	80	5	0.972	0.555	0.845	0.799	0.628	0.8344
Flat bar	4	1200	160	10	95	6	0.972	0.428	0.804	0.809	0.629	0.8218
Flat bar	5	1200	300	10	40	4	1.822	1.735	0.501	0.531	0.280	0.5017
Flat bar	6	1200	300	10	50	4	1.822	1.353	0.589	0.553	0.402	0.5168
Flat bar	7	1200	300	10	90	6	1.822	0.557	0.793	0.693	0.528	0.7564
Flat bar	8	1200	300	10	110	6	1.822	0.432	0.752	0.717	0.396	0.7348
Flat bar	9	1200	300	10	130	8	1.822	0.321	0.754	0.736	0.336	0.7307
Flat bar	10	1200	300	8	40	4	2.278	1.691	0.450	0.423	0.286	0.4516
Flat bar	11	1200	300	8	80	5	2.278	0.651	0.629	0.611	0.572	0.6281
Flat bar	12	1200	300	8	95	6	2.278	0.490	0.629	0.650	0.351	0.6529
Flat bar	13	1200	300	8	110	6	2.278	0.407	0.615	0.669	0.304	0.6493
Flat bar	14	1200	300	8	130	8	2.278	0.306	0.629	0.690	0.266	0.6569
Flat bar	15	1200	300	6	65	5	3.037	0.783	0.518	0.483	0.516	0.5173
Flat bar	16	1200	300	6	80	5	3.037	0.599	0.518	0.533	0.358	0.5246
Flat bar	17	1200	300	6	95	6	3.037	0.455	0.528	0.574	0.259	0.5321
Flat bar	18	1200	300	6	110	6	3.037	0.380	0.524	0.594	0.231	0.5391
Flat bar	19	1200	300	6	130	8	3.037	0.291	0.544	0.614	0.208	0.566
Flat bar	20	1200	160	8	40	4	1.215	1.327	0.725	0.721	0.425	0.7248
Flat bar	21	1200	160	8	65	5	1.215	0.680	0.825	0.757	0.613	0.8265
Flat bar	22	1200	160	8	80	5	1.215	0.528	0.785	0.775	0.622	0.8137
Flat bar	23	1200	160	8	95	6	1.215	0.410	0.791	0.788	0.623	0.8008
Flat bar	24	1200	160	6	80	5	1.620	0.498	0.752	0.730	0.527	0.7731
Flat bar	25	1200	160	6	95	6	1.620	0.391	0.717	0.747	0.427	0.7574
Flat bar	26	900	300	5	40	4	3.644	1.134	0.328	0.344	0.406	0.3286
Flat bar	27	900	300	5	50	4	3.644	0.850	0.431	0.406	0.472	0.4331
Flat bar	28	900	300	5	65	5	3.644	0.557	0.531	0.485	0.277	0.5259
Flat bar	29	900	300	5	80	5	3.644	0.428	0.541	0.522	0.217	0.5452
Flat bar	30	900	300	5	95	6	3.644	0.327	0.566	0.549	0.190	0.5593
Flat bar	31	900	300	5	110	6	3.644	0.274	0.562	0.562	0.180	0.5747
Flat bar	32	900	300	5	130	8	3.644	0.212	0.589	0.574	0.169	0.6017
Flat bar	33	900	300	7	80	5	2.603	0.470	0.628	0.617	0.300	0.6169
Flat bar	34	900	300	7	95	6	2.603	0.355	0.651	0.645	0.253	0.6284
Flat bar	35	900	300	7	110	6	2.603	0.296	0.645	0.657	0.235	0.6426
Flat bar	36	900	300	7	130	8	2.603	0.224	0.658	0.670	0.219	0.6701
Flat bar	37	900	300	8	50	4	2.278	0.968	0.469	0.535	0.514	0.4895
Flat bar	38	900	300	8	65	5	2.278	0.637	0.688	0.614	0.545	0.6327
Flat bar	39	900	300	8	80	5	2.278	0.488	0.683	0.651	0.349	0.6528
Flat bar	40	900	300	8	95	6	2.278	0.368	0.705	0.678	0.287	0.6495
Flat bar	41	900	300	8	110	6	2.278	0.306	0.694	0.690	0.266	0.6569
Flat bar	42	900	300	8	130	8	2.278	0.230	0.703	0.702	0.246	0.6786
Mean									0.639	0.636	0.380	0.6383
Standard deviation									0.122	0.115	0.147	0.1225
Coefficient of variation									0.191	0.181	0.387	0.1919

ID: identification.

panel surrounded by successive longitudinal or transverse stiffeners) and six to seven elements are also considered along the web of the stiffener. Figure 2 shows a typical example of a discretized stiffened plate model.

Mechanical properties of the material

The material properties were taken from the Aalberg et al.[13] experiments. Young's modulus E and Poisson's ratio ν of the material are 70.475 GPa and 0.3 respectively. The stress–strain relationship of the aluminium alloy is shown in Figure 3(a). The breadth of the HAZ is assumed to be 50 mm in the plate and 25 mm in the stiffener web, at the plate–stiffener junction (Figure 3(b)).

Extent of the model, boundary and loading conditions

A double-span single-stiffener model or, in other words, a double-span double-bay model (ABCD in Figure 4) was chosen for the analysis of the collapse behaviour of stiffened aluminium plates.[36] The boundary conditions of the analysed plates are as follows.

1. Symmetry conditions are imposed at the same x coordinate along the longitudinal edges of the model (i.e. along AB and CD).
2. Symmetry conditions are imposed at the same y coordinate along the transverse edges in the model (i.e. along AD and BC).

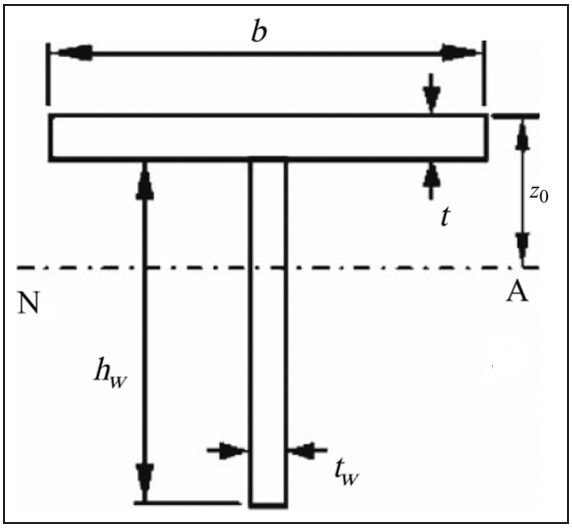

Figure 1. The cross-sectional geometry of stiffened aluminium plates.
A and N: neutral axis.

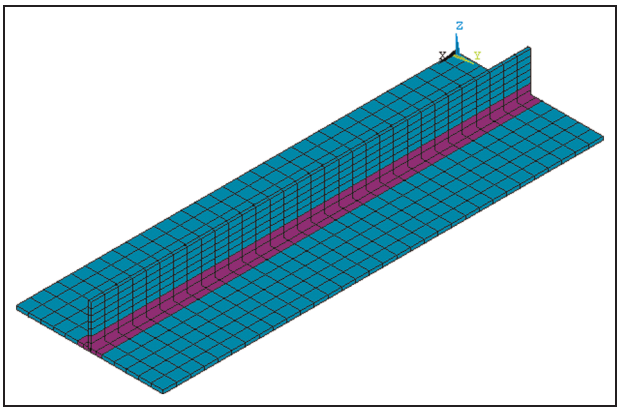

Figure 2. Typical example of a meshed model.

3. Although transverse frames are not modelled, the out-of-plane deformation of the plate is restrained along its junction line with the transverse frame.
4. To consider the plate continuity, the in-plane movement of the plate edges in their perpendicular directions is assumed to be uniform.

After producing the initial deflection in the stiffened plate, longitudinal compression in exerted on the stiffened plate.

Initial imperfections

The initial deflection of the local plate panels is in a very complex mode.[37] Although it is assumed to be in a buckling mode in some research studies, the real shape of the initial deflection can be considered to be in a so-called thin-horse mode.[38,39] There are also different methods in order to establish such a complex thin-horse mode of the initial deflection in the plate and stiffener elements of the stiffened plates. One of the methods recently adopted by some researchers in a benchmark study on the ultimate strength analysis of stiffened aluminium plates[19] is selected in this paper. According to this experience, lateral pressure was applied first on the stiffened plate model and a linear elastic finite element analysis was carried out. Such an analysis was repeated in a trial-and-error sequence of calculations until the deflection of plate reaches the average value given by

$$W_{0\max} = c\beta^2 t \tag{1}$$

The value of the coefficient c depends on the level of the initial deflection. The maximum magnitude $W_{0\max}$ of the initial deflection is taken from the work of Varghese[40] as

$$W_{0\max} = 0.05\beta^2 t \tag{2}$$

After satisfying this condition, data information including the coordinates of the nodal points, element coordinates and boundary conditions were extracted and transferred to a new finite element mesh. The new model was used for a non-linear finite element analysis of the stiffened plate subjected to in-plane compression. The procedure generating the initial deflection is shown schematically in Figure 5.

In addition to the initial deflections in both the plate and the stiffener, the material softening in the HAZ and also the welding residual stresses are taken into account.

Zha–Moan tests

A total of 21 stiffened aluminium panels were tested by Zha and Moan.[17] The nominal geometrical dimensions of the test specimens are shown in Figure 6. Zha and Moan prepared two sets of test specimens were prepared: one set made of aluminium alloy AA5083-H116 and the other set made of aluminium alloy AA6082-T6. The plate thickness, the stiffener height and the web thickness were varied in each set. The end plates of each specimen were machined in a parallel way in order to achieve uniform application of the load. A test rig was designed as shown in Figure 6.

The longitudinal edges of the specimens were free, while the stiffened panel was simply supported along the transverse boundaries. The test specimen was mounted in a vertical position. The axial compressive loading was applied at the upper end of the specimen through a rigid loading set, while the reaction force was carried by the lower-end support set. Before testing, the initial imperfections of the stiffened panels were measured. During the tests, the axial compressive load was applied by slowly imposing a displacement; subsequently the deformation of the stiffened plate was measured. The simply supported boundary conditions were provided by a steel cylinder bearing, with a diameter of 30 mm, as shown in Figure 6. More details have been given in the paper by Zha and Moan.[17]

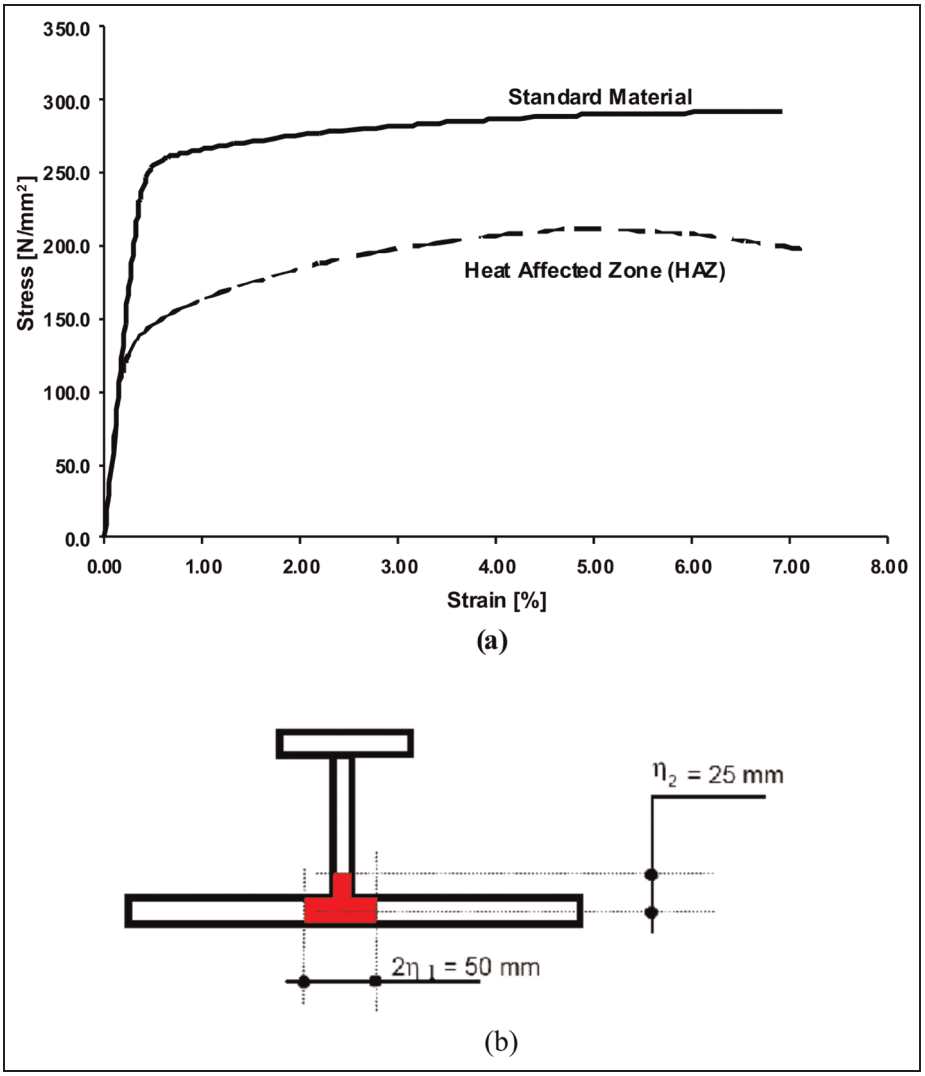

Figure 3. (a) The stress–strain behaviour of the material; (b) the extent of the HAZ in both the plate and the stiffener.

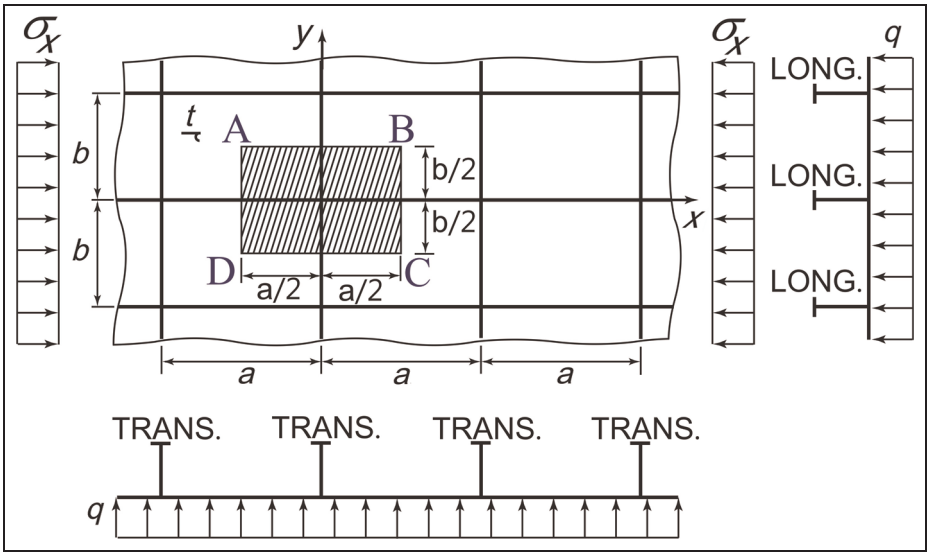

Figure 4. The extent of the continuous stiffened plate models for analysis.
LONG.: longitudinal; TRANS.: transverse.

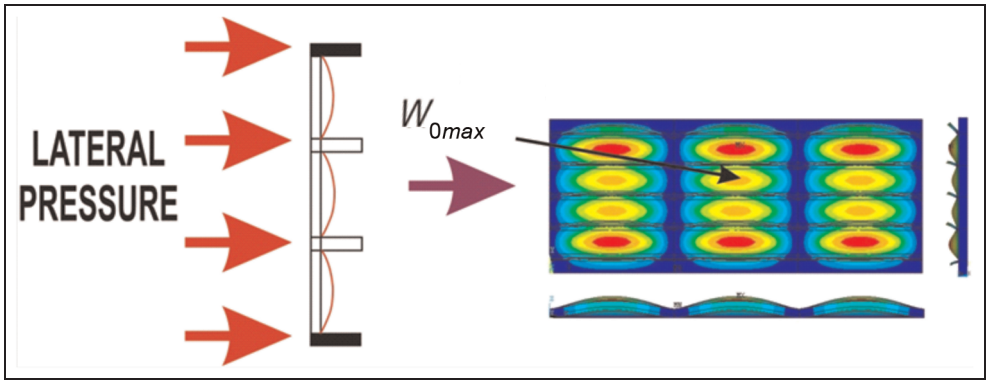

Figure 5. Procedure to generate the initial deflection.

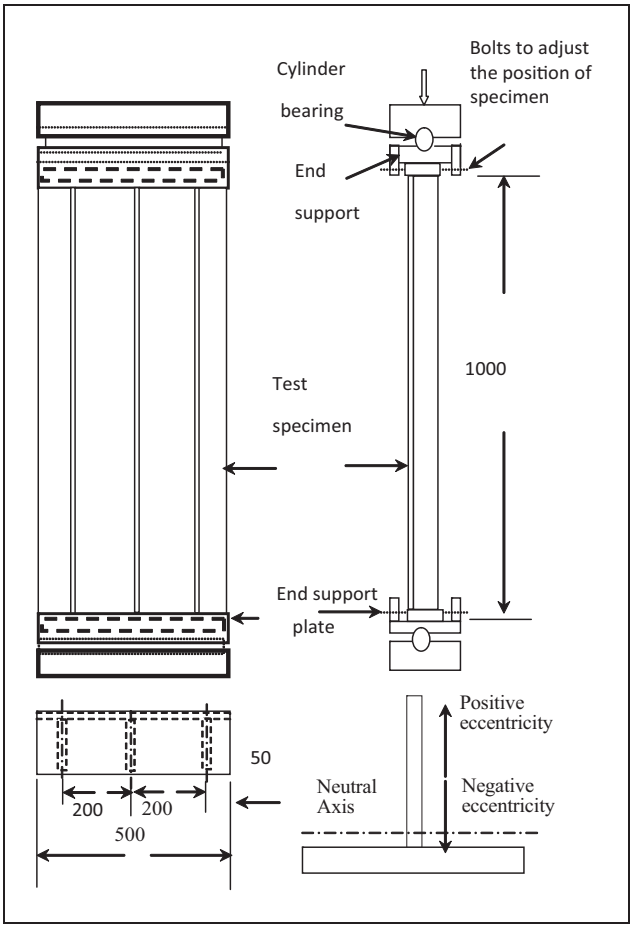

Figure 6. Test rig set-up with the test specimen used by Zha and Moan[17] (all dimensions are in millimetres).

The test specimens used by Zha and Moan were designed to collapse because of the torsional buckling of the stiffeners. However, the torsional buckling of the stiffeners interacted with the local panel buckling of the plates, as observed from the test specimens with a thin plate thickness. Significant torsional deformation of the stiffeners was observed when the axial compressive load was increased beyond 70% of the ultimate load. The number of half-waves in the collapse modes was influenced by the initial imperfection of the stiffeners. Because of the variations in the material properties and the geometric dimensions of the test specimens, the buckling and plastic collapse behaviour varied during the tests. Typical behaviour of the specimens was described by using specimens EA2, A7, A12 and A16 as examples. Among the test specimens used by Zha and Moan,[17] two specimens A7 and A16 were chosen for validation purposes.

In addition to performing tests, Zha and Moan also performed numerical simulations by ABAQUS. The same tests on specimens A7 and A16 were simulated using ANSYS by the present authors. Figure 7 and Figure 8 represent the collapse modes of specimen A7 and specimen A16 respectively, as obtained from the tests and numerical simulations. Also, the load-end shortening curves for these two specimens are shown in Figure 9 and Figure 10 respectively. As can be seen, when the HAZ is not considered, the corresponding load-end shortening curves show an upper ultimate strength which is higher than that obtained in the tests. When considering the HAZ, the ultimate strength predicted by ABAQUS[17] and ANSYS differ by about 5% and 8% respectively from that obtained experimentally for specimen A7. The difference between the tests and the numerical results for specimen A16 becomes much smaller when using either ABAQUS or ANSYS. More or less the same collapse modes with similar features are obtained experimentally or numerically for both specimen A7 (Figure 7) and specimen A16 (Figure 8).

Ultimate strength and collapse behaviour

A series of elastic–plastic large-deflection finite element analyses was performed on all the models described earlier. Relationships between the average stress σ and the average strain ε for all the stiffened plates under longitudinal compression were obtained. For rapid access to the results that are of greater importance to the present study, the numerical values of the ultimate strength of stiffened plates under longitudinal compression are summarized in the twelfth column of Table 1. Also, the collapse modes at the ultimate strength level and at the final stage of calculations for some typical

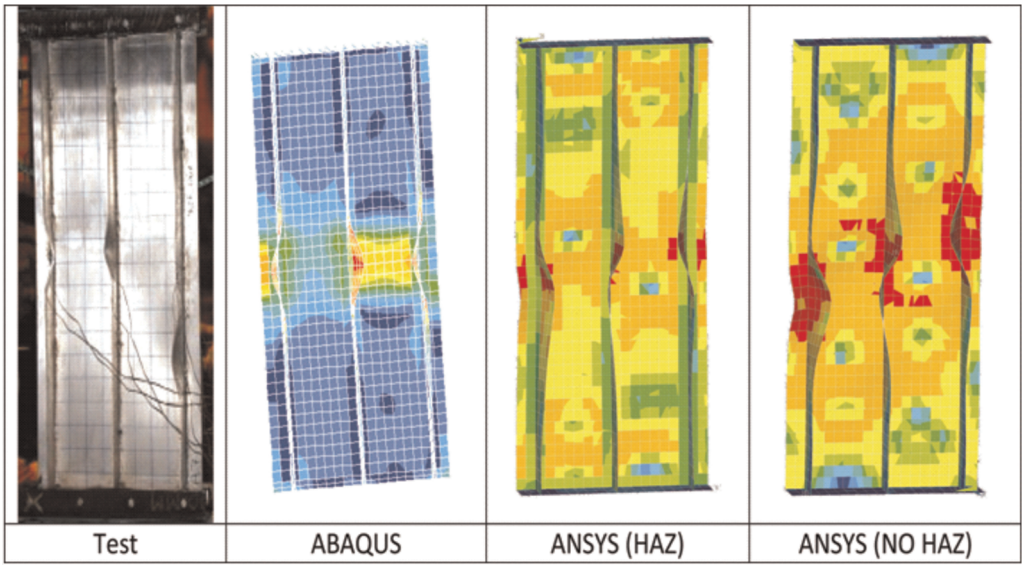

Figure 7. Experimentally and numerically obtained collapse modes of specimen A7 (material, AA5083-H116; the test and ABAQUS results considering the HAZ were taken from the work of Zha and Moan[17]; the ANSYS results were obtained by the present authors).
HAZ: heat-affected zone.

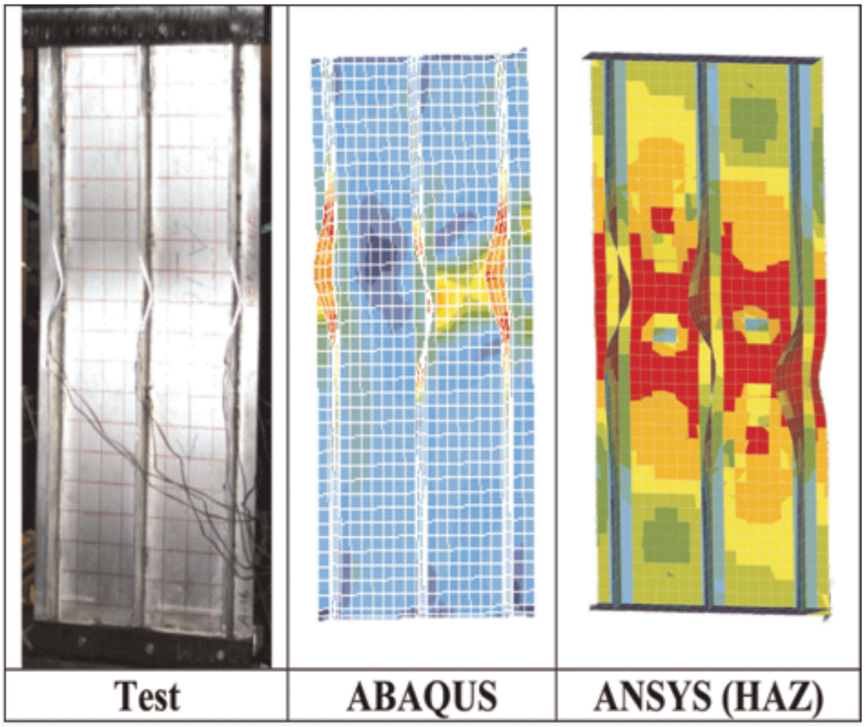

Figure 8. Experimentally and numerically obtained collapse modes of specimen A16 (material, AA6082-T6; the test and ABAQUS results considering the HAZ were taken from the work of Zha and Moan[17]; the ANSYS results were obtained by the present authors).
HAZ: heat-affected zone.

models under axial compression are shown in Table 2. For stiffened plates with flat-bar stiffeners, the collapse mode occurs in a buckling mode under pure in-plane compression (Table 2). At the final stage of the calculations, it is observed that unloading (stress removal) takes place in some parts of the stiffened plates while, in the remaining parts, localized plastic deformations are accumulated (Table 2). Also, severe tripping of the longitudinal stiffeners is observed at the line of the transverse supporting members. For a more thorough

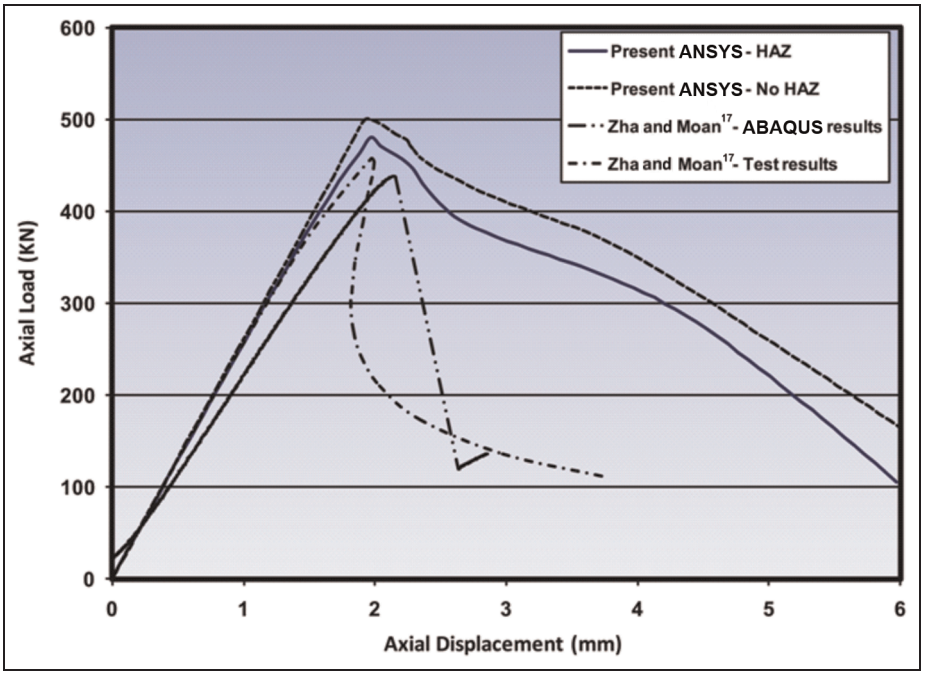

Figure 9. Load-end shortening curves for specimen A7.
HAZ: heat-affected zone.

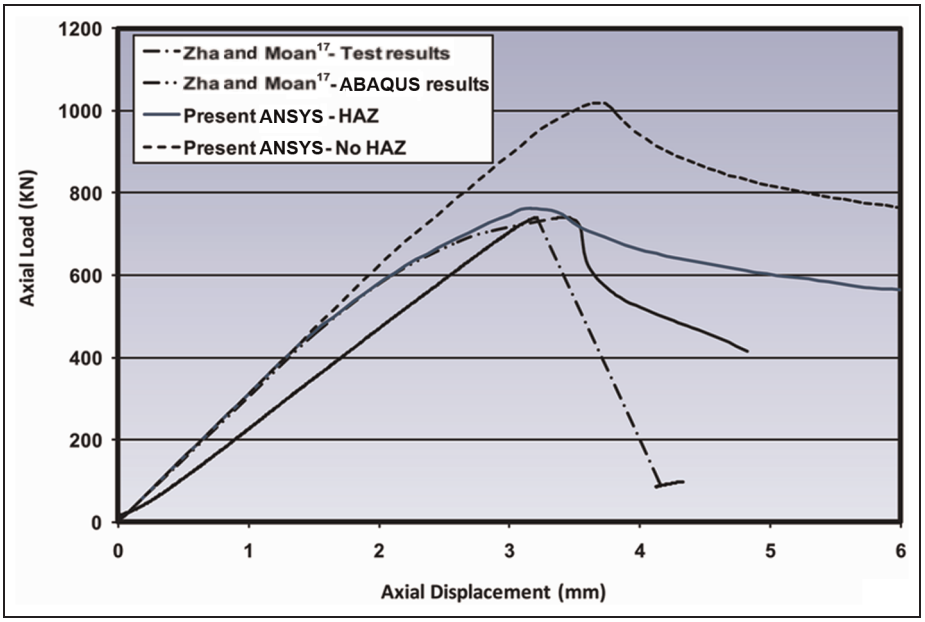

Figure 10. Load-end shortening curves for specimen A16.
HAZ: heat-affected zone.

insight into the different aspects of the structural behaviour of stiffened aluminium plates, reference should be made to the work of Khedmati et al.[28]

Empirical formulation

General form of the formulation

Paik[23] derived closed-form empirical ultimate strength formulae for stiffened aluminium plate structures under axial compressive loads by a regression analysis of experimental and numerical databases. The formulation derived by Paik[23] for the case of aluminium plate with flat-bar stiffeners was

$$\frac{\sigma_{Ult}}{\sigma_{Yseq}} = \begin{cases} \min\left(\frac{1}{\sqrt{2.500 + 0.084\beta^2 - 0.588\lambda^2 + 0.069\lambda^2\beta^2 + 1.217\lambda^4}}\right) \leqslant \frac{1}{\lambda^2} \\ \min\left(\frac{1}{\sqrt{-16.297 + 17.716\beta + 18.776\lambda - 22.507\lambda\beta}}\right) \end{cases} \tag{3}$$

where

Table 2. Ultimate strength mode and final collapse mode of some typical continuous stiffened aluminium plates obtained by the FEM.

ID	Ultimate strength mode (magnified 10×)	End of the analysis (magnified 3×)
37	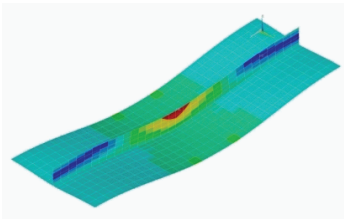	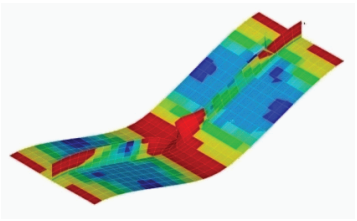
38	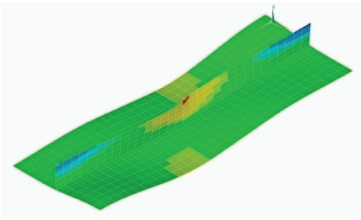	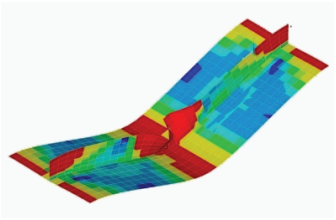
39	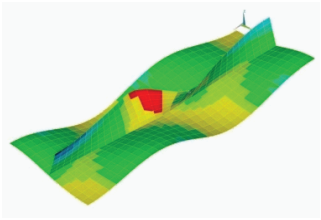	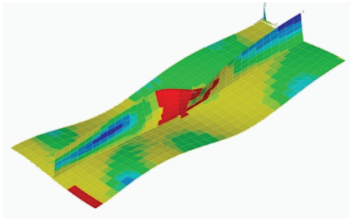
40	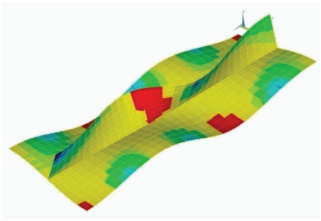	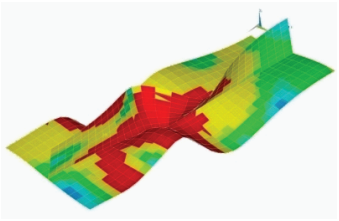
41	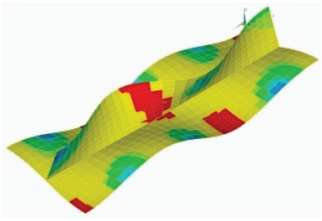	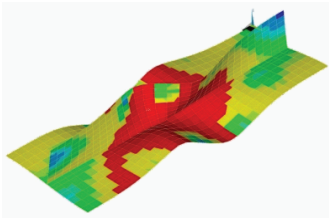
42	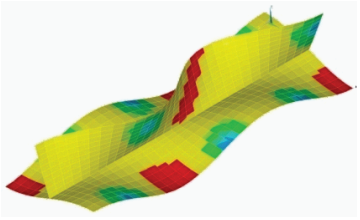	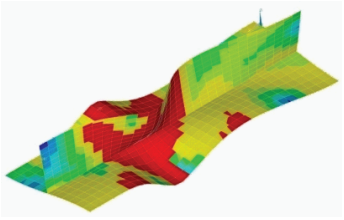

ID: identification.

$$\beta = \frac{b}{t}\sqrt{\frac{\sigma_{Yp}}{E}} \tag{4}$$

$$\lambda = \frac{a}{\pi r}\sqrt{\frac{\sigma_{Yseq}}{E}} \tag{5}$$

$$r = \sqrt{\frac{I}{bt + h_w t_w + b_f t_f}} \tag{6}$$

$$I = \frac{bt^3}{12} + bt\left(z_0 - \frac{t}{2}\right)^2 + \frac{h_w^3 t_w}{12} + h_w t_w\left(z_0 - t - \frac{h_w}{2}\right)^2 + \frac{b_f t_f^3}{12} + b_f t_f\left(t + h_w t_w + \frac{t_f}{2} + z_0\right)^2 \tag{7}$$

$$z_0 = \frac{0.5bt^2 + h_w t_w(t + 0.5h_w) + b_f t_f(t + h_w + 0.5t_f)}{bt + h_w t_w + b_f t_f} \tag{8}$$

$$\sigma_{Yseq} = \frac{\sigma_{Yp} bt + \sigma_{Ys}(h_w t_w + b_f t_f)}{bt + h_w t_w + b_f t_f} \tag{9}$$

Ultimate strength of uniaxially compressed stiffened aluminium plates with flat-bar stiffeners

In this paper, the same form of ultimate strength formulation as described by equation (3) is used. Different coefficients are derived on the basis of the developed numerical database in order to estimate the ultimate strength of stiffened aluminium plates with a flat-bar stiffener cross-section under in-plane compression.

Regression analysis is applied to the numerical data listed in Table 1. The same form of the ultimate strength formulation as given by equation (3) is kept throughout the regression analysis. The coefficients are updated so as to give suitable estimates of the ultimate strength for the case under consideration. The equation obtained as a result is

$$\frac{\sigma_{Ult}}{\sigma_{Yseq}} = \frac{1}{\sqrt{1.3551 + 0.1107\beta^2 + 0.0814\lambda^2 + 0.3423\beta^2\lambda^2 - 0.2031\lambda^4}} \leqslant \frac{1}{\lambda^2} \tag{10}$$

Equation (10) is used to predict the ultimate strengths of all the models in Table 1. These values are placed in the thirteenth column of Table 1. Also, the predicted ultimate strengths of the models using equation (3) are listed in the fourteenth column of Table 1. Figure 11(a) shows the accuracy of Paik's empirical formula versus that of the present empirical formula for the analysed models. As can be observed, the value of the ultimate strength prediction using the present empirical formula is generally greater than the prediction using Paik's empirical formula. Also, relatively good agreement is observed in Figure 11(b) between the values of the ultimate strengths based on the FEM and those predicted by the present empirical formula (equation (10)).

The derived formulation is also found to be very effective in terms of time. Estimation of the ultimate strength of continuous stiffened aluminium plates using the presented formulation takes a few milliseconds. In contrast, modelling of a continuous stiffened aluminium plate with all details, using any commercial finite element code such as ANSYS, for an expert and skilled user takes about two or three working days. This is because the central processing unit time for its analysis for capturing the value of the ultimate strength including post-processing jobs is about 30–40 min.

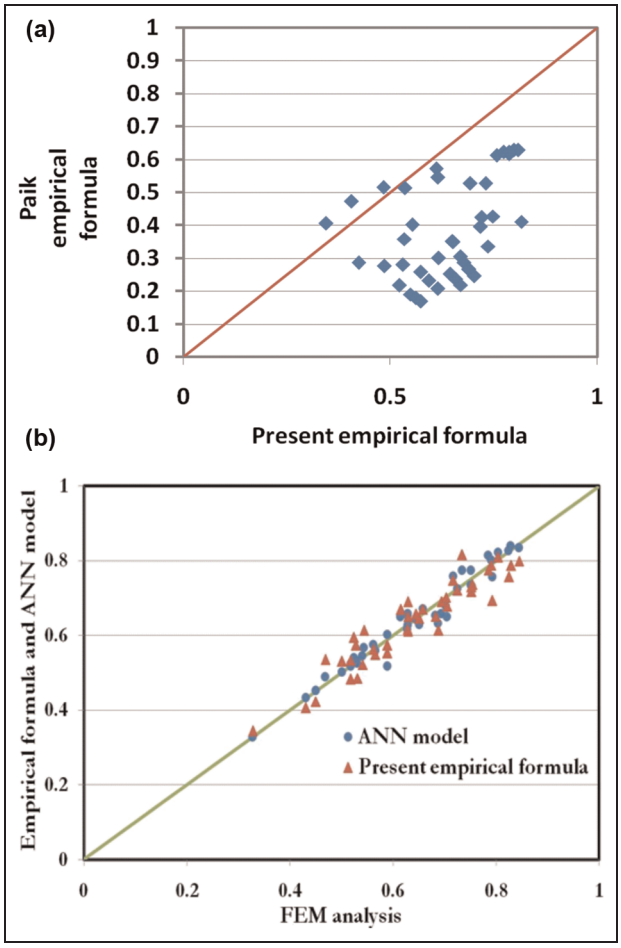

Figure 11. (a) Comparison of the non-dimensionalized ultimate strength values obtained using Paik's empirical formula versus those values predicted using the present empirical formula. (b) Comparison of the non-dimensionalized ultimate strength values obtained using the FEM versus those values predicted using the present empirical formula and the ANN model.
ANN: artificial neural network; FEM: finite element method.

Artificial neural networks

General concept

ANNs have been developed as generalizations of the mathematical models of biological nervous systems.[41] An ANN is a mathematical representation of interconnected computing elements (or neurons) arranged in layers, which process information by their response to external inputs, in an analogous way to the central nervous system. The attractiveness of ANNs is their potential to learn from input–output data sets and their ability to approximate any continuous non-linear function to any arbitrary degree of accuracy, using a feed-forward process.[42] A typical ANN model and also the basic neuron in it are illustrated in Figure 12. ANN models have three layers: the input layer, the hidden layer(s) and the output layer. The input and output layers consist of vectors of the input variables and the output variables.

The hidden layer(s) consist of neurons, which are each connected via weight vectors to each of the nodes in the input layer and to each of the neurons in the output layer. Each neuron consists of weights whose function is to scale the inputs to the transfer function and biases that control the location of the decision boundaries. The neuron functions by summing the inputs $\boldsymbol{p}$ multiplied by their respective weights $\mathbf{W}$ and adding a bias $\boldsymbol{B}$. This sum of products is operated on by a transfer function that serves to limit the maximum value of the summation.[43] The outputs of each neuron pass through a non-linear activation function which is called a transfer function (f in Figure 12). The main objective of the transfer function is that the output of this function is bounded above and below and is continuous and differentiable everywhere. The corresponding output of a general ANN model is given by

$$\boldsymbol{A} = f_1(\mathbf{W}_2 f_2(\mathbf{W}_1 \times \boldsymbol{p} + \boldsymbol{B}_1) + \boldsymbol{B}_2) \quad (11)$$

Typical transfer functions used in the MATLAB neural network toolbox are described in Table 3.

Developing a neural network consists of two major steps, namely 'training' (or learning) and 'testing' (or verification). During the training process, combinations of known input–output data ('training sets') are repeatedly presented to the ANN and the weights $\mathbf{W}_1$ and $\mathbf{W}_2$ associated with each neuron are adjusted until the specified input provides the desired output. Through these adjustments, the ANN 'learns' the correct input–output response behaviour. This training process is usually accomplished by using some particular algorithm in which a cost function, specified as the sum of squared errors between the true output and the output produced by the network, is minimized. When the cost function approaches a minimum, the network is considered to have converged. Minimization of the cost function can be achieved in different ways. The most popular technique is the back-propagation (BP) algorithm. After training, the ANN is then subjected to the verification stage in which other combinations of known input–output data are introduced ('testing sets') in order to estimate the residual error. Based on the performance of the trained ANN, further adjustments may be

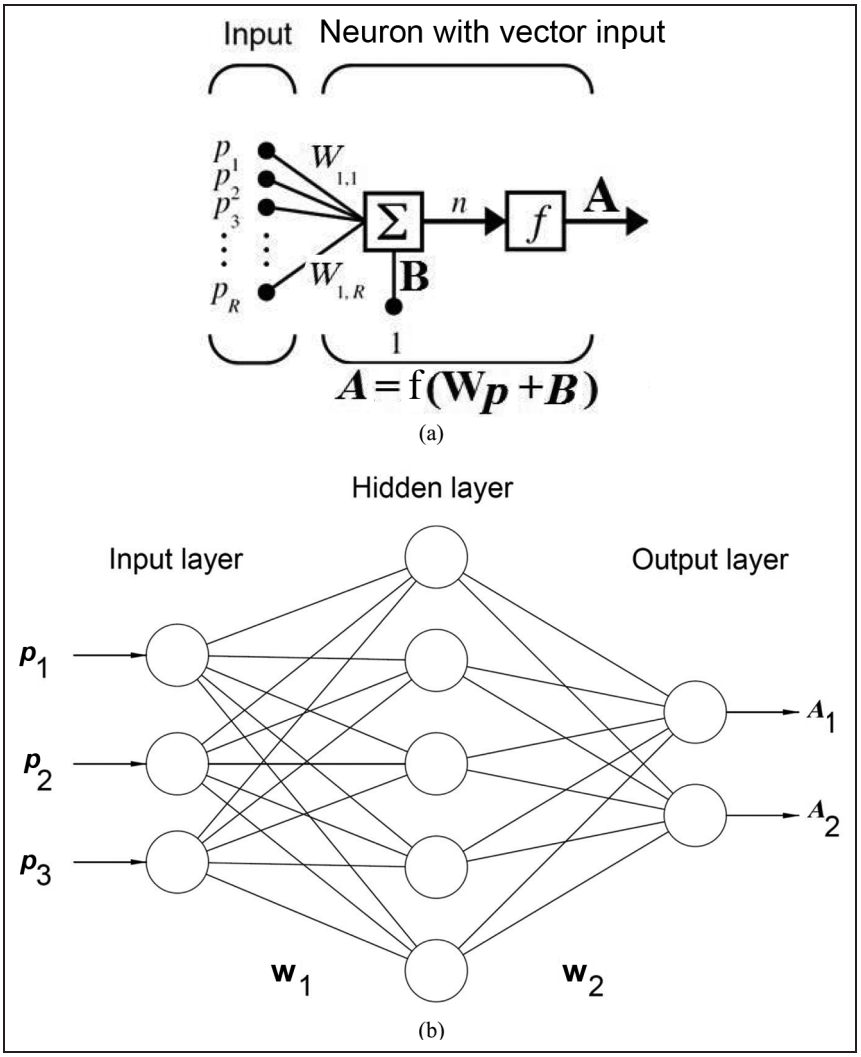

Figure 12. (a) Basic neuron; (b) typical ANN model.

Table 3. Typical transfer functions.

Name	Function	Output (where n is the input)	
Tangent sigmoid	tansig	$\frac{2}{1+\exp(-2n)}-1$	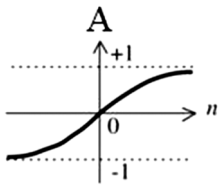
Logarithm sigmoid	logsig	$\frac{1}{1+\exp(-n)}$	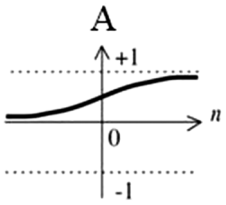
Linear	purelin	n	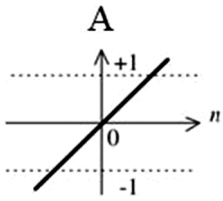

appropriate to make the model more accurate and/or robust.[42] In this study the performance function of training is the mean squared error (MSE) given by

$$\mathrm{MSE} = \frac{1}{Q}\sum_{k=1}^{Q}[T(k) - A(k)] \tag{12}$$

The training set of a typical ANN consists of 60–80% of the known data and does not necessarily span the entire system space. The remaining 20–40% of the data are used for testing and validation.[44]

Structure of the ANN model

The multi-layer feedforward network is the most commonly used network architecture with the BP algorithm. Feedforward networks often have one or more hidden layers. Multiple layers of neurons with non-linear transfer functions allow the network to learn non-linear and linear relationships between the input and the output vectors. Application of feedforward BP neural networks to predict the ultimate strength has been performed by Pu and co-workers.[32,33]

In this study, the ANN is trained and used to approximate the ultimate strength of stiffened aluminium plates under uniaxial compression. Also, Neural Network Toolbox V6.0 of MATLAB® mathematical software was used. A three-layer BP ANN model with a logarithm sigmoid (logsig) transfer function at the hidden layer (function f_2 in equation (11)) and a linear (purelin) transfer function at the output layer (function f_1 in equation (11)) is used. The data are divided into training, validation and testing subsets, i.e. 60%, 20% and 20% respectively of the data. The input and target variables are randomly loaded into the workspace. In the next few sections, first a comparison between different types of BP algorithm is made, and then the number of neurons in each layer and optimization of the ANN model are discussed.

Number of neurons in different layers

As mentioned above, a three-layer ANN model was selected and, thus, the number of neurons in each layer is to be defined. The number of neurons in the input layer and the number of neurons in the output layer are equal to the number of input variables and the number of output variables respectively. The geometrical characteristics and the material properties of stiffened plates are factors affecting their ultimate strengths. The effects of these parameters are summarized into and represented by two variables including the slenderness parameter β of the plate and the column slenderness parameter λ of the stiffened plate. Therefore, only two input variables are used in the ANN model and as a result there are two neurons in the input layer. The desired output of the ANN model is the ultimate strength of stiffened plates, and thus only one output datum and one neuron would exist in the output layer. It should be noted that, in the calculation of the output data from equation (11), the input data and the output data must be normalized. The normalization is performed using

Table 4. Comparison of BP algorithms with 10 neurons in the hidden layer.

Back-propagation algorithm	Function	MSE	Number of epochs	R^2	Best linear equation
Broyden– Fletcher–Goldfarb–Shanno quasi-Newton back propagation	trainbfg	0.00096	10	0.9388	$y = 0.87x + 0.0866$
Bayesian regulation back propagation	trainbr	0.0146	11	0.9586	$y = 0.87x + 0.088$
Conjugate gradient back propagation with Powell–Beale restarts	traincgb	0.00114	6	0.9694	$y = 1.1x + 0.1$
Conjugate gradient back propagation with Fletcher–Reeves updates	traincgf	0.00158	4	0.9433	$y = 0.84x + 0.081$
Conjugate gradient back propagation with Polak–Ribière updates	traincgp	0.00151	9	0.9133	$y = 0.88x + 0.44$
Gradient-descent back propagation	traingd	0.0126	6	0.5835	$y = 0.33x + 0.39$
Gradient descent with momentum back propagation	traingdm	0.0143	373	0.4767	$y = 0.42x + 0.15$
Gradient descent with adaptive learning rate back propagation	traingda	0.00205	194	0.8938	$y = 0.80x + 0.074$
Gradient descent with momentum and adaptive learning rate back propagation	traingdx	0.00175	124	0.9071	$y = 0.88x + 0.12$
One-step secant back propagation	trainoss	0.00461	6	0.8643	$y = 0.80x + 0.0866$
Resilient back propagation	trainrp	0.00144	23	0.9626	$y = 1.0x + 0.0013$
Scaled conjugate gradient back propagation	trainscg	0.00176	14	0.9530	$y = 0.99x + 0.0025$
Levenberg–Marquardt back propagation	trainlm	0.000415	6	0.9714	$y = 0.97x + 0.031$

MSE: mean squared error.

$$X_{nor} = \frac{(Y_{max} - Y_{min})(X - X_{min})}{X_{max} - X_{min}} + Y_{min} \quad (13)$$

for the input data, while the inverse is carried out for the output data. Y_{min} and Y_{max} represent the limits of a boundary in which the values of X are to be normalized. Herein, $Y_{min} = -1$ and $Y_{max} = +1$.

The number of neurons in the hidden layer has a significant effect on the accuracy of the ANN models. In the next section, the number of neurons in the hidden layer is optimized on the basis of the MSE of the ANN models in selected BP algorithms.

Selection of the back-propagation algorithm

There are several types of BP algorithm in MATLAB. In this section, a comparison between different training algorithms is made in order to select the best BP training algorithm. All algorithms have 10 neurons in their hidden layers. The comparison is shown in Table 4. The Levenberg–Marquardt back-propagation algorithm (LMA) has a smaller MSE than the other BP algorithms. Therefore, in the present study, the LMA is selected to be the training algorithm.

Optimization of the ANN model

Optimization of the ANN model is performed on the basis of the criterion of the minimum value of the MSE at the training stage. Figure 13 illustrates the dependence between the number of neurons in the hidden layer and the MSE for the LMA. As can be seen, the MSE is initially equal to 0.0007844 when three neurons are used. On the other hand, it decreases to a value of 0.0002854 when eight neurons are applied. With a further increase in the number of hidden neurons, the MSE starts to increase. Hence, the neural network with eight hidden neurons is chosen as the best case. Figure 14 shows the optimized ANN structure. It has a three-layer ANN, with a logsig transfer function at the hidden layer with eight neurons and a purelin transfer function at the output layer. The weights and biases for the ANN architecture shown in Figure 14 are given in the form of matrices and vectors in Table 5. Consequently, the ANN model for prediction of the ultimate strength can be described using equation (11). The output $\boldsymbol{A}$ of this equation is the normalized ultimate strength (the ultimate strength of stiffened plate divided by the yield strength of the material used). It should be noted that the matrices **IW** and **LW** appearing in both Table 5 and Figure 14 are equal to $\mathbf{W}_1$ and $\mathbf{W}_2$ respectively in equation (11). **LW**, **IW**, $\boldsymbol{B}_1$ and $\boldsymbol{B}_2$ in equation (11) are obtained from Table 5. f_1 and f_2 in

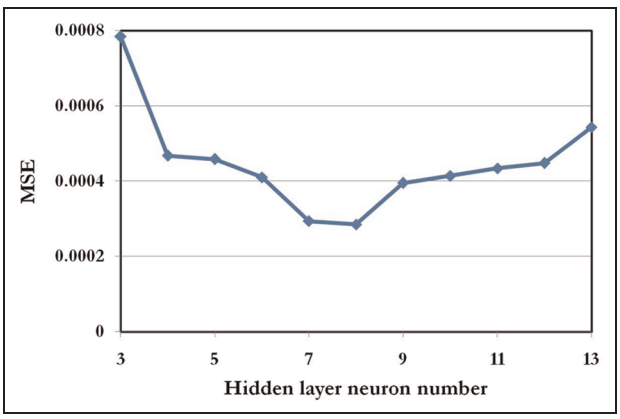

Figure 13. Relationship between the MSE and the number of neurons in the hidden layer.
MSE: mean squared error.

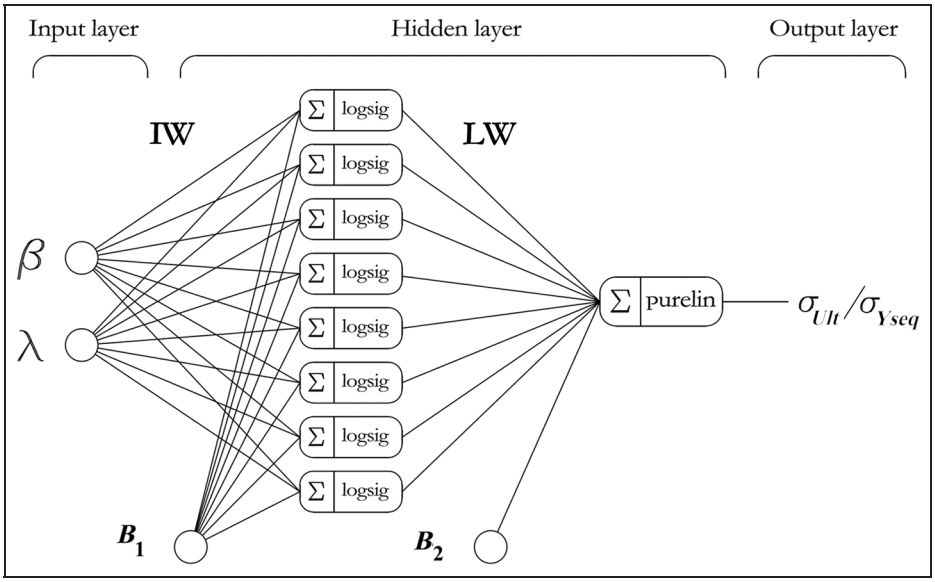

Figure 14. Optimal architecture of the ANN model.

equation (11) are the logsig transfer function and the purelin transfer function respectively. In this equation, $\boldsymbol{p}$ is a vector containing the β and λ values of the stiffened plate ($\boldsymbol{p}$[1,1] is β and $\boldsymbol{p}$[2,1] is λ).

In MATLAB, after simulating and creating the ANN model, a regression analysis between the ANN outputs and the corresponding targets is performed (Figure 15). In Figure 15, the horizontal axis represents the target values as obtained from the FEM analyses and the vertical axis shows the outputs of the ANN model. This figure contains two lines. The dashed line is the perfect fit $y = x$, and the solid line is the best fit with the linear equation $y = x + 0.0077$, where the correlation coefficient $R^2 = 0.96975$.

Numerical example

A numerical example is described in order to show how to use the developed ANN model to estimate the ultimate strength of uniaxially loaded stiffened aluminium plates. The characteristics of the stiffened aluminium plate under consideration are given in the first six columns of Table 6. The values of the quantities β and λ for such a stiffened plate can be obtained as

$$\beta = 1.822,\ \lambda = 1.735$$

From the database shown in Table 1, the values extracted are

$$\beta_{min} = 0.972, \beta_{max} = 3.644$$
$$\lambda_{min} = 0.212, \lambda_{max} = 1.735$$

and also

$$\left(\frac{\sigma_{Ult}}{\sigma_{Yseq}}\right)_{FEM,\,min} = \left(\frac{\sigma_{Ult}}{\sigma_{Yseq}}\right)_{min} = 0.328]$$

Table 5. Optimal values of the weights and biases obtained during network training with the LMA.

Input weight matrix	$\mathbf{IW} = \begin{bmatrix} -7.2431 & 2.4351 \\ -6.3454 & -5.1084 \\ 4.1711 & -5.3849 \\ -9.4993 & -1.2379 \\ 4.1805 & 6.9310 \\ 4.3188 & 3.0842 \\ -0.3934 & -8.4850 \\ -2.9511 & -7.3600 \end{bmatrix}$
Bias vector	$\boldsymbol{B}_1 = [9.4056 \quad 5.3181 \quad -3.1154 \quad 1.1592 \quad -2.3843 \quad 0.8344 \quad -5.8375 \quad -7.7618]^T$
Layer weight vector	$\mathbf{LW} = [-1.6325 \quad 1.8277 \quad -0.1201 \quad -1.0053 \quad 1.0532 \quad -2.4405 \quad -0.6391 \quad 0.5569]$
Bias scalar	$\boldsymbol{B}_2 = [1.8081]$

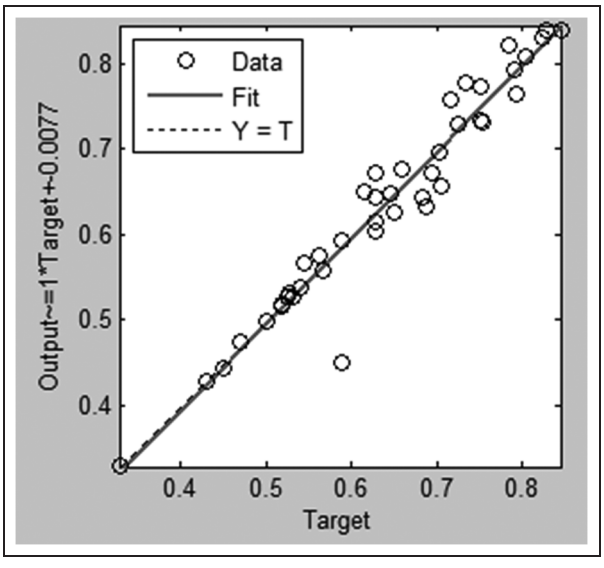

Figure 15. Comparison between the target and the output of the optimized ANN model.

Table 6. Numerical example.

Stiffener type	a (mm)	b (mm)	t (mm)	h_w (mm)	t_w (mm)	β	λ	$\left(\frac{\sigma_{Ult}}{\sigma_{Yseq}}\right)_{FEM}$	$\left(\frac{\sigma_{Ult}}{\sigma_{Yseq}}\right)_{Empirical\ formula}$	$\left(\frac{\sigma_{Ult}}{\sigma_{Yseq}}\right)_{Paik}$	$\left(\frac{\sigma_{Ult}}{\sigma_{Yseq}}\right)_{ANN}$
Flat bar	1200	300	10	40	4	1.822	1.735	0.501	0.531	0.280	0.501

$$\left(\frac{\sigma_{Ult}}{\sigma_{Yseq}}\right)_{FEM,max} = \left(\frac{\sigma_{Ult}}{\sigma_{Yseq}}\right)_{max} = 0.845$$

Now the values of the parameters are to be normalized using equation (13). The procedure is

$$\begin{aligned}\beta_{nor} &= \frac{[1-(-1)](\beta-\beta_{min})}{\beta_{max}-\beta_{min}} + (-1)\\ &= \frac{2(1.822-0.972)}{3.644-0.972} - 1\\ &= -0.3638\end{aligned}$$

and also

$$\begin{aligned}\lambda_{nor} &= \frac{[1-(-1)](\lambda-\lambda_{min})}{\lambda_{max}-\lambda_{min}} + (-1)\\ &= \frac{2(1.735-0.212)}{1.735-0.212} - 1\\ &= 1\end{aligned}$$

from which the vector $\boldsymbol{p}$ is obtained as

$$\boldsymbol{p} = \begin{bmatrix}\beta_{nor}\\ \lambda_{nor}\end{bmatrix} = \begin{bmatrix}-0.3638\\ 1\end{bmatrix} \quad (14)$$

Putting $\boldsymbol{p}$ as obtained from equation (14) into equation (11) and also considering the values of $\mathbf{W}_1 = \mathbf{IW}$, $\mathbf{W}_2 = \mathbf{LW}$, $\boldsymbol{B}_1$ and $\boldsymbol{B}_2$ as given in Table 5, the normalized value of $\sigma_{Ult}/\sigma_{Yseq}$ is obtained as –0.3282. Recalling equation (13), we may write

$$\left(\frac{\sigma_{Ult}}{\sigma_{Yseq}}\right)_{nor} = \frac{[1-(-1)]\left[\sigma_{Ult}/\sigma_{Yseq} - \left(\sigma_{Ult}/\sigma_{Yseq}\right)_{min}\right]}{\left(\sigma_{Ult}/\sigma_{Yseq}\right)_{max} - \left(\sigma_{Ult}/\sigma_{Yseq}\right)_{min}} + (-1)$$

or

$$-0.3282 = \frac{[1-(-1)]\left(\sigma_{Ult}/\sigma_{Yseq} - 0.328\right)}{0.845-0.328} + (-1)$$

Finally, it can be found that $\sigma_{Ult}/\sigma_{Yseq} = 0.501$. This value is given in the twelfth column of Table 6.

Comparison between the empirical formulae and the ANN prediction

The ultimate strength of the considered stiffened aluminium plates under study are also assessed using the ANN model. The results are given in the last column of Table 1. Also a comparison of the ultimate strength values obtained by the FEM and by the ANN model is shown in Figure 11(b). As can be understood from Figure 11(b), the ANN model gives a better estimation of the ultimate strength of stiffened aluminium plates under uniaxial compression than does the regression-based empirical formulation.

Conclusions

In this paper, first a closed-form ultimate compressive strength formula is derived for stiffened aluminium plates by regression analysis of the computed results. Subsequently, ANN methodology is applied to predict the ultimate strength of stiffened aluminium plates under uniaxial compression. The proposed ANN model is trained and cross-validated using the existing database. It is found that the ANN model can produce a more accurate prediction of the ultimate strength of stiffened aluminium plates than the existing empirical formula can. This demonstrates the capacity of the ANN method to establish successfully a functional relationship between the input parameters and the output parameters.

The present study is limited to the stiffened aluminium plates with flat-bar stiffeners and subjected to uniaxial in-plane compression. Other stiffener types, such as L- or T-bar stiffeners and other load cases, such as lateral pressure or transverse compression, will have different effects on the strength of the stiffened aluminium plates. Developing other ANN models in order to predict the ultimate strength of stiffened aluminium plates considering other types of stiffener or other loading conditions is an interesting topic for further future research.

Funding

This research received no specific grant from any funding agency in the public, commercial or not-for-profit sectors.

References

1. Murray NW. Buckling of stiffened panels loaded axially and in bending. *Struct Engng* 1973; 51(8): 285–301.
2. Dorman AP and Dwight JB. Tests on stiffened compression panels and plate panels. In: *International conference on steel box girder bridges*, London, UK, 13–14 February 1973, pp. 63–75. London: Institution of Civil Engineers.
3. Smith CS. Compressive strength of welded steel ship grillages. *Trans R Inst Nav Archit* 1975; 117: 325–47.
4. Dow RS. Testing and analysis of a 1/3-scale welded steel frigate model. In: CS Smith and RS Dow (eds) *Advances in marine structures – 2*. Barking, Essex: Elsevier Applied Science, 1991, pp.749–773.

5. Ghavami K. Experimental study of stiffened plates in compression up to collapse. *J Constructional Steel Res* 1994; 28(2): 197–222.
6. Sherbourne AN, Liaw CY and Marsh C. Stiffened plates in uniaxial compression. *IABSE* 1971; 31: 145–177.
7. Moolani FM and Dowling PJ. Ultimate load behaviour of stiffened plates in compression steel plates structures. In: PJ Dowling, JE Harding and PA Frieze (eds) *International conference on steel plated structures*, London, UK, July 1976, pp.51–88. London: Crossby Lockwood Staples.
8. Guedes Soares C and Soreide TH. Behaviour and design of stiffened plates under predominantly compressive loads. *Int Shipbuilding Prog* 1983; 30(341): 13–27.
9. Bonello MA, Chryssanthopoulos MK and Dowling PJ. Ultimate strength design of stiffened plates under axial compression and bending. *Mar Structs* 1993; 6: 533–552.
10. Chen Q, Zimmerman TJE, DeGeer D and Kennedy BW. Strength and stability testing of stiffened plate components. Report SSC-399, Ship Structure Committee, Washington, DC, USA, 1997.
11. Clarke JD and Narayanan, R. Buckling of aluminium alloy stiffened plate ship structure. In: *International conference on steel and aluminium structures*, Cardiff, UK, 8–10 July 1987, pp. 81–92. Barking, Essex: Elsevier Applied Science.
12. Aalberg A, Langseth M and Larsen PK. Stiffened aluminium panels subjected to axial compression. *Thin Walled Structs* 2001; 39: 861–885.
13. Aalberg A, Langseth M and Malo KA. Ultimate strength of stiffened aluminium plates. Report, Department of Structural Engineering, Norwegian University of Science and Technology, Trondheim, Norway, 1998.
14. Kristensen QHH and Moan T. Ultimate strength of aluminium plates under biaxial loading. In: *5th international conference on fast sea transportation*, Seattle, WA, USA, 31 August–2 September 1999. Jersey City, NJ: Society of Naval Architects and Marine Engineers.
15. Zha Y, Moan T and Hanken E. Experimental and numerical study of torsional buckling of stiffeners in aluminium panels. In: *10th annual international offshore and polar engineering conference,* Seattle, WA, USA, 27 May–2 June 2000, pp. 249–255. Cupertino, CA: International Society of Offshore and Polar Engineers.
16. Zha Y, Moan T and Hanken E. Ultimate strength of stiffened aluminium panels with predominantly torsional failure modes. *Thin-Walled Structs* 2001; 39: 631–648.
17. Zha Y and Moan T. Experimental and numerical prediction of collapse of flat bar stiffeners in aluminium panels. *J Struct Engng* 2003; 129(2): 160–168.
18. Hopperstad OS, Langseth M and Hanssen L. Ultimate compressive strength of plate elements in aluminium, correlation of finite element analyses and tests. *Thin-Walled Structs* 1998; 29: 31–46.
19. Rigo P, Sarghiuta R, Estefen S et al. Sensitivity analysis on ultimate strength of aluminium stiffened panels. *Marine Structs* 2003; 16: 437–468.
20. Paik JK, Hughes OF, Hess PE et al. Ultimate limit state design technology for aluminium multi-hull ship structures. *Trans SNAME* 2005; 113: 270–305.
21. Paik JK, Thayamballi AK, Ryu JY et al. The statistics of weld induced initial imperfections in aluminium stiffened plate structures for marine applications. *Int J Marit Engng* 2006; 148(4): 19–63.
22. Collette MD. The impact of fusion welds on the ultimate strength of aluminium structures. In: *10th international symposium on practical design of ships and other floating structures*, Houston, TX, USA, 1–5 October 2007. Houston, TX: American Bureau of Shipping.
23. Paik JK. Empirical formulations for predicting the ultimate compressive strength of welded aluminium stiffened panels. *Thin-Walled Structures* 2007; 45: 171–184.
24. Sielski RA. Research needs in aluminium structure. *Ships Offshore Structs* 2008; 3(1): 57–65.
25. Paik JK, Andrieu C and Cojeen HP. Mechanical collapse testing on aluminium stiffened plate structures for marine applications. *Mar Technol* 2008; 45(4): 228–240.
26. Paik JK, Thayamballi AK, Ryu JY et al. Mechanical collapse testing on aluminium stiffened panels for marine applications. Report SSC-451, Ship Structure Committee, Washington, DC, USA, 2008.
27. Paik JK. Buckling collapse testing of friction stir welded aluminium stiffened plate structures. Report SR-1454, Ship Structure Committee, Washington, DC, USA, 2009.
28. Khedmati MR, Zareei MR and Rigo P. Sensitivity analysis on the elastic buckling and ultimate strength of continuous stiffened aluminium plates under combined in-plane compression and lateral pressure. *Thin-Walled Structs* 2009; 47(11): 1232–1245.
29. Khedmati MR, Zareei MR and Rigo P. Empirical formulations for estimation of ultimate strength of continuous stiffened aluminium plates under combined in-plane compression and lateral pressure. *Thin-Walled Structs* 2010; 48(3): 274–289.
30. Zanic V, Andric J and Prebeg P. Design environment for structural design: application to modern multideck ships. *Proc IMechE Part M: J Engineering in the Maritime Environment* 2009; 223(1): 105–120.
31. Pu Y, Mesbahi E and Elhewy AH. ANN-based response surface method and its application to ultimate strength of plates. In: *15th annual international offshore and polar engineering conference*, Seoul, Republic of Korea, 19–24 June 2005, pp. 752–758. Cupertino, CA: International Society of Offshore and Polar Engineers.
32. Pu Y and Mesbahi E. Application of artificial neural networks to evaluation of ultimate strength of steel panels. *Engng Structs* 2006; 28: 1190–1196.
33. Ok D, Pu Y and Incecik A. Artificial neural networks and their application to assessment of ultimate strength of plates with pitting corrosion. *Ocean Engng* 2007; 34: 2222–2230.
34. Sadovský Z and Guedes Soares C. Artificial neural network model of the strength of thin rectangular plates with weld induced initial imperfections. *Reliability Engng System Safety* 2011; 96: 713–717.
35. *ANSYS user's manual, version 7.1*. Houston, TX: Swanson Analysis Systems Inc., 2003.
36. Yao T, Fujikubo M, Yanagihara D and Irisawa M. Consideration on FEM modelling for buckling/plastic collapse analysis of stiffened plates (in Japanese). *Trans West-Japan Soc Nav Archit* 1998; 85: 121–128.
37. Ueda Y and Yao T. The influence of complex initial deflection on the behaviour and ultimate strength of rectangular plates in compression. *J Constructional Steel Res* 1985; 5: 265–302.
38. Fujikubo M, Yao T, Khedmati MR et al. Estimation of ultimate strength of continuous stiffened panel under

combined transverse thrust and lateral pressure, Part 1: continuous plate. *Mar Structs* 2005; 18: 383–410.
39. Fujikubo M, Harada S, Yao T et al. Estimation of ultimate strength of continuous stiffened panel under combined transverse thrust and lateral pressure, Part 2: continuous stiffened panel. *Mar Structs* 2005; 18: 411–417.
40. Varghese B. *Buckling/plastic collapse strength of plates and stiffened plates under combined loads*. DrEng Thesis, Hiroshima University, Hiroshima, Japan, 1998.
41. Abraham A, Sydenham P and Thorn R. *Handbook of measuring system design (artificial neural networks)*. New Work: John Wiley, 2005.
42. Rao Z and Alvarruiz F. Use of an artificial neural network to capture the domain knowledge of a conventional hydraulic simulation model. *J Hydro Informatics* 2007; 9(1): 15–24.
43. Demuth H, Beale M and Hagan M. *Neural Network Toolbox™ user's guide*. Natick, MA: The MathWorks Inc., 2008.
44. Lucon PA and Donovan RP. An artificial neural network approach to multiphase continua constitutive modelling. *Composites, Part B, Engng* 2007; 38(3): 817–823.

Appendix I

Notation

a	length of the local plate panel
$\boldsymbol{A}$	output data from the artificial neural network model
b	overall breadth of the plate
b_f	flange breadth of the longitudinal stiffener
$\boldsymbol{B}_i$	bias of the artificial neural network model ($i = 1, 2$)
c	coefficient of the maximum magnitude of the initial deflection
E	Young's modulus
h_w	height of the longitudinal stiffener web
I	moment of inertia of the stiffener with the attached plating
$\mathbf{IW}$	input weight matrix
$\boldsymbol{LW}$	layer weight vector
$\boldsymbol{p}$	vector of the normalized input parameters
q	lateral pressure
Q	variable number in the output
r	radius of gyration of the stiffener with the attached plating $= \sqrt{I/A}$
t	plate thickness $= t_p$
t_f	flange thickness of the longitudinal stiffener
t_w	thickness of the longitudinal stiffener web
T	target data
W_{0max}	maximum magnitude of the initial deflection
$\mathbf{W}_i$	weighting matrices in the artificial neural network model ($i = 1, 2$, $\mathbf{W}_1 = \mathbf{IW}$ and $\mathbf{W}_2 = \mathbf{LW}$)
β	slenderness parameter of the plate $= (b/t)\sqrt{\sigma_{Yp}/E}$
ε	average strain
λ	column slenderness parameter of the stiffened plate $= (a/\pi r)\sqrt{\sigma_{Yseq}/E}$
ν	Poisson's ratio
σ	average stress
σ_{Ult}	ultimate strength
σ_{Yp}	yield stress of the plate
σ_{Yseq}	equivalent yield stress for the stiffened plate